Inorganic Chemistry

Article

pubs.acs.org/IC

# Transformation of Barium−Titanium Chloro−Alkoxide Compound to $BaTiO_3$ Nanoparticles by $BaCl_2$ Elimination

Magdalena Kosińska-Klähn,[†] Łukasz John,[†] Anna Drąg-Jarząbek,[†] Józef Utko,[†] Rafał Petrus,[†] Lucjan B. Jerzykiewicz,[†] and Piotr Sobota*[,†,‡]

[†]Faculty of Chemistry, University of Wrocław, 14 F. Joliot-Curie, 50-383 Wrocław, Poland

[‡]Research & Development Centre Novasome, 5 Olsztyńska, 51-423 Wrocław, Poland

Supporting Information

**ABSTRACT:** In this Article, we present how the molecular precursor of binary oxide material having an excess of alkali earth metal can be transformed to the highly phase pure $BaTiO_3$ perovskite. Here, we synthesized and compared two barium−titanium complexes with and without chloride ligands to determine the influences of different ligands on the phase purity of binary oxide nanoparticles. We prepared two barium−titanium complexes, i.e., $[Ba_4Ti_2(\mu_6\text{-}O)(OCH_2CH_2OCH_3)_{10}(HOCH_2CH_2OCH_3)_2(HOOCCPh_3)_4]$ (**1**) and $[Ba_4Ti_2(\mu_6\text{-}O)(\mu_3,\eta_2\text{-}OCH_2CH_2OCH_3)_8(\mu\text{-}OCH_2CH_2OCH_3)_2(\mu\text{-}HOCH_2CH_2OCH_3)_4Cl_4]$ (**2**). The barium−titanium precursors were characterized using elemental analysis, infrared and nuclear magnetic resonance spectroscopies, and single-crystal X-ray structural analysis, and their thermal decomposition products were compared. The complex **1** decomposed at 800 °C to give a mixture of $BaTiO_3$ and $Ba_2TiO_4$, whereas **2** gave a $BaCl_2/BaTiO_3$ mixture. Particles of submicrometer size (30−50 nm) were obtained after leaching of $BaCl_2$ from the raw powder using deionized water. Preliminary studies of barium titanate doped with $Eu^{3+}$ sintered at 900 °C showed that the dominant luminescence band arose from the strong electric dipole transition, $^5D_0-^7F_2$.

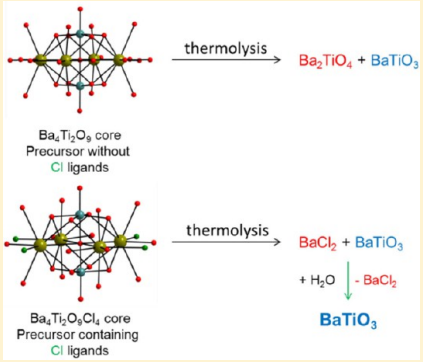


## INTRODUCTION

The rapidly growing importance of technologically attractive binary oxides has resulted in intensive study and development of suitable synthetic routes. Specific precursors and the use of suitable synthetic methods are needed for the preparation of metal oxides in various forms, with different sizes, shapes, and morphologies. Chemical vapor deposition (CVD) and sol−gel processes are general and affordable approaches to the preparation of metal oxides, and different types of materials have been developed using different precursors, and based on the underlying chemistry. All the available techniques yield materials with excellent properties, but they can have some disadvantages such as high costs. These can easily be overcome, e.g., by process optimization and its technology.[1]

For many years, because of their commercial significance, metal alkoxides have been considered to be good single-source precursors for oxide ceramic materials. Considerable effort has gone into precursor choice, and several reports on this topic have been published.[2−5] Halide−alkoxides are the least explored class of precursors, because they tend to promote HCl evolution during thermolysis and form multicomponent phases, which contaminate the final product; this is undesirable technologically and in terms of product purity. However, some mono- and heterometallic chloride−alkoxides have been used to obtain highly pure metal oxides. Epifani et al. described a chloro−alkoxide route to transition-metal oxides. In their work, tungsten, molybdenum, and vanadium chloro−methoxides were prepared by methanolysis of $WCl_6$, $MoCl_5$, and $VCl_4$, respectively. Studies have clearly shown that the precursor structures evolve continuously to the final $WO_3$, $MoO_3$, and $V_2O_5$ structures.[6−8] Although many homometallic halo−alkoxides have been successfully used to obtain halide-free oxide nanoparticles,[6,8] the synthesis of heterometallic halo−alkoxides has been less explored, and heterometallic and ionic complex formation have not been reported.[9,10] Mazharand and co-workers synthesized the heterobimetallic chloride−alkoxo molecular precursor $[Zn_7(OAc)_{10}(\mu\text{-}OH)_6Cu_5(dmae)_4Cl_4]$ (dmae = *N*,*N*-dimethylamino)ethanolate; OAc = acetate) for the deposition of metal−oxide thin-films of $Cu_5Zn_7O_{12}$.[11] Also, Mishra et al. reported the synthesis of a novel molecular precursor by a convenient reaction between a metal chloride with a metal alkoxide, which underwent facile conversion to a halide-free spinodal form of $Ta^{5+}$-doped $TiO_2-SnO_2$.[12]

Among technologically important binary oxides, perovskite $BaTiO_3$ is particularly important, because of its wide range of applications.[13] This well-known ferroelectric material can be used as a dielectric ceramic for capacitors and piezoelectric materials for microphones and other transducers,[14,15] in nonlinear optics for thin films with electro-optical modulation to frequencies over 40 GHz,[16] as uncooled sensors for thermal cameras, and as a key component in new energy-storage systems for use in electric vehicles. It is also an attractive host lattice for doping with lanthanide ions, and these doped

**Received:** October 25, 2013
**Published:** January 10, 2014





dx.doi.org/10.1021/ic402987n | *Inorg. Chem.* 2014, 53, 1630−1636

materials have many applications, for example, in lasers, field-emission displays, and integrated light-emission devices.[17]

In this study, on the basis of reports of the alcoholysis of chloride transition-metal complexes, we investigated the technologically important barium−titanium mixed-metal oxide systems. Our aim was to synthesize and compare barium−titanium complexes with and without chloride ligands. We then explored the possibility of obtaining phase-pure double-oxide systems from crystalline heterometallic alkoxides, and the best way to avoid impurities, enabling easy conversion of solid-state spinel to a perovskite material. We also investigated whether the replacement of some O,O′-type ligands by chloride ligands is a good idea. This Article describes the method for synthesizing mixed metal oxides from heterometallic clusters. We report a facile synthesis of a highly phase-pure $BaTiO_3$ nanopowder, which is an efficient host matrix for $Eu^{3+}$ ions.

## EXPERIMENTAL SECTION

**General Procedures and Methods.** Reactions were conducted under nitrogen using standard Schlenk techniques. Solvents were prepared as follows: toluene was distilled from Na/benzophenone; hexanes were distilled from $P_2O_5$. Barium (pieces, 99%), potassium (pieces, 99%), bis(cyclopentadienyl)titanium(IV) dichloride ($Cp_2TiCl_2$ powder, 98%), 2-methoxyethanol (anhydrous liquid, 99.8%), triphenylacetic acid ($Ph_3CCOOH$ powder, 99%), and europium(III) oxide ($Eu_2O_3$ powder 99.9%) were purchased from Aldrich and used without further purification. Microanalyses were conducted using a 2400 CHNS Vario EL III (Elementar) elemental analyzer. The concentrations of metal ions were determined by inductively coupled plasma atomic emission spectrometry using an ARL 3410 sequential spectrometer (Fisons Instruments). Fourier-transform infrared (FT-IR) spectra were recorded as Nujol mulls using a Bruker 66/s FT-IR spectrometer. Nuclear magnetic resonance (NMR) spectroscopy was performed using a Bruker ADVANCE 500 MHz spectrometer. Thermogravimetric analysis−differential thermal analysis (TGA−DTA) was performed in an air atmosphere, using a SETSYS 16/18 system (SETARAM), at a heating rate of 5 °C $min^{-1}$. Thermal decompositions were performed using an NT 1313 furnace with a KXP3+ thermostat (NEOTHERM). Samples were thermolyzed in atmospheric air. The thermolysis products were characterized by powder X-ray diffraction (XRD), using a Bruker D8 ADVANCE diffractometer equipped with a copper lamp ($\lambda_{CuK\alpha}$ = 1.5418 Å). Measurements were performed in the range $2\theta$ = 10−90°, with $2\theta$ steps of 0.016° and a counting time of 0.3 s. The powder morphologies were examined by high-resolution transmission electron microscopy (TEM), using a FEI Tecnai $G^2$ 20 X-TWIN microscope operated at 200 kV, providing 0.25 nm resolution, equipped with an EDAX microanalyzer, and scanning electron microscopy (SEM), using a Hitachi S-3400N microscope equipped with a Thermo Noran System SIX energy-dispersive X-ray spectroscopy (EDS) system. Nitrogen porosimetry was performed at 77 K using a Micromeritics ASAP 2020 M system. The specific surface area ($S_{BET}$) was calculated using the Brunauer−Emmett−Teller (BET) method. The mesopore size distribution was determined using the Barrett−Joyner−Halenda (BJH) method from the desorption branch. Pore size distributions were calculated using the BJH model, based on nitrogen desorption isotherms. Photoluminescence spectra were recorded using an FSL920 spectrofluorimeter (Edinburgh Instruments) with a 450 W Xe lamp and a photomultiplier tube, operated in the range 185−870 nm. The luminescence spectra resolution was 0.2 nm.

**Synthesis of $[Ba_4Ti_2(\mu_6\text{-}O)(OCH_2CH_2OCH_3)_{10}(HOCH_2CH_2OCH_3)_2(OOCCPh_3)_4]$ (1).** A Schlenk flask was charged with $Cp_2TiCl_2$ (0.823 g; 3.30 mmol), metallic barium (0.908 g; 6.61 mmol), 2-methoxyethanol (20 mL; 19.3 g; 0.253 mol), and toluene (20 mL). The solution was vigorously stirred at room temperature until all the metal was consumed (1 h). Potassium triphenyl acetate ($Ph_3CCOOK$) (2.16 g; 6.61 mmol) was then added (obtained by simple stoichiometric reaction of metallic potassium and triphenylacetic acid in toluene at room temperature). The mixture was stirred for 24 h and then filtered. The filtrate was reduced under a vacuum to 10 mL, and then hexane (5 mL) was added, forming a layer over the filtrate, and was left at −15 °C. Colorless crystals of **1** grew within a few days. Overall yield: 3.81 g; 1.40 mmol; 85%. Calcd for $C_{116}H_{146}O_{33}Ti_2Ba_4$ (MW, 2713.42): C, 51.35; H, 5.42; Ti, 3.53; Ba, 20.24. Found: C, 51.41; H, 5.39; Ti, 3.47; Ba, 20.12. IR ($cm^{-1}$, Nujol mull): 3053 (br), 2923 (vs), 2714 (w), 1596 (s), 1492 (m), 1459 (s), 1377 (s), 1355 (s), 1250 (m), 1197 (m), 1151 (s), 1122 (s), 1071 (s), 1021 (s), 966 (w), 927 (w), 899 (s), 834 (s), 804 (w), 793 (w), 738 (s), 699 (s), 672 (m), 642 (m), 624 (m), 606 (m), 552 (s), 461 (s), 396 (s), 355 (s), 316 (m) 183 (m), 125 (s). $^1$H NMR (500 MHz, $CD_3OD$, 298 K, ppm): $\delta$ = 3.27 (s, 36H, $HOCH_2CH_2OCH_3$), 3.34−3.40 (m, 24H, $HOCH_2CH_2OCH_3$), 3.50−3.58 (m, 24H, $HOCH_2CH_2OCH_3$), 4.74 (br, 2H, $HOCH_2CH_2OCH_3$), 7.02−7.20 (m, 60H, phenyl groups). $^{13}$C{$^1$H} NMR (500 MHz, $CD_3OD$, 298 K, ppm): $\delta$ = 57.83 (s, 12C, $HOCH_2CH_2OCH_3$), 60.60 (s, 12C, $HOCH_2CH_2OCH_3$), 73.66 (s, 12C, $HOCH_2CH_2OCH_3$), 63.44 (s, 4C, $C\text{-}Ph_3$), 125.38, 126.73, 130.57, 146.28 (s, 72C, phenyl groups), 175.01 (s, 4C, COOH). GC/MS: CpH (MW, 66), CpH dimer (traces), 1-methylcyclohexa-1,4-diene (traces), cyclopentene (traces).

**Synthesis of $[Ba_4Ti_2(\mu_6\text{-}O)(\mu_3,\eta^2\text{-}OCH_2CH_2OCH_3)_8(\mu\text{-}OCH_2CH_2OCH_3)_2(\mu\text{-}HOCH_2CH_2OCH_3)_4Cl_4]$ (2).** *Method A.* A Schlenk flask was charged with $Cp_2TiCl_2$ (1.00 g; 2.63 mmol), $Ba(OCH_2CH_2OCH_3)_2$ (1.52 g; 5.26 mmol), 20 mL of 2-methoxyethanol (19.30 g; 0.25 mol), and toluene (20 mL). The mixture was vigorously stirred for 4 h. The resulting yellow solution was filtered, concentrated under vacuum to 20 mL, and left to crystallize at −15 °C. After 72 h, colorless crystals were collected, washed with *n*-hexane (3 × 5 mL), and dried under vacuum. The filtrate volume was reduced to 10 mL; after standing overnight at −15 °C, another portion of crystalline material was obtained. Overall yield: 2.24 g; 1.20 mmol; 60%. Calcd for $C_{42}H_{102}O_{29}Cl_4Ti_2Ba_4$ (MW, 1858.15): C, 27.15; H, 5.53; Cl, 7.63; Ti, 5.15; Ba, 29.56. Found: C, 27.11; H, 5.57; Cl, 7.57; Ti, 5.14; Ba, 29.86. IR ($cm^{-1}$, Nujol mull): 3412 (br), 2924 (vs), 2854 (s), 1644 (w), 1461 (s), 1377 (s), 1287 (w), 1237 (m), 1198 (m), 1146 (s), 1120 (s), 1067 (s), 1021 (s), 986 (w), 935 (w), 908 (m); 838 (s); 696 (s), 590 (s), 560 (s), 495 (s), 459 (s), 393 (s). $^1$H NMR (500 MHz, $CDCl_3$, 298 K, ppm): $\delta$ = 5.14 (s, 4H, $HOCH_2CH_2OCH_3$), 4.18 (br, 16H, $OCH_2CH_2OCH_3$), 4.05 (t, 4H, $OCH_2CH_2OCH_3$, $J_{H-H}$ = 5 Hz), 3.72 (t, 8H, $HOCH_2CH_2OCH_3$, $J_{H-H}$ = 5 Hz), 3.65 (br, 16H, $OCH_2CH_2OCH_3$), 3.52 (s, 12H, $HOCH_2CH_2OCH_3$), 3.51 (s, 24H, $OCH_2CH_2OCH_3$), 3.48 (t, 8H, $HOCH_2CH_2OCH_3$, $J_{H-H}$ = 5 Hz), 3.32 (t, 4H, $OCH_2CH_2OCH_3$, $J_{H-H}$ = 5 Hz), 3.26 (s, 6H, $OCH_2CH_2OCH_3$). $^{13}$C{$^1$H} NMR (500 MHz, $CDCl_3$, 298 K, ppm): $\delta$ = 77.46 (s, 4C, $HOCH_2CH_2OCH_3$), 76.51 (s, 2C, $OCH_2CH_2OCH_3$), 73.76 (s, 8C, $OCH_2CH_2OCH_3$), 67.74 (s, 2C, $OCH_2CH_2OCH_3$), 64.58 (s, 4C, $HOCH_2CH_2OCH_3$), 61.00 (s, 8C, $OCH_2CH_2OCH_3$), 59.82 (s, 8C, $OCH_2CH_2OCH_3$), 59.57 (s, 4C, $HOCH_2CH_2OCH_3$), 58.59 (s, 2C, $OCH_2CH_2OCH_3$). GC/MS: CpH (MW, 66), CpH dimer (traces), 1-methylcyclohexa-1,4-diene (traces), cyclopentene (traces).

*Method B.* Complex **2** was also obtained by reacting $Cp_2TiCl_2$ (1.00 g; 4.02 mmol), metallic barium (1.45 g; 10.56 mmol), 20 mL of 2-methoxyethanol (19.30 g; 0.25 mol), and toluene (20 mL) (one-pot pathway). A procedure analogous to that used in method A gave colorless block crystals of **2** after 4 d. Overall yield: 52%. Elemental analysis and spectroscopic data confirmed that the obtained compound was complex **2**.

**XRD Determinations of Structures.** Crystals were mounted on glass fibers and then flash-frozen to 100(2) K (Oxford Cryosystem-Cryostream Cooler). Preliminary examination and intensity data collection were carried out with a Kuma KM4CCD $\kappa$-axis diffractometer with graphite-monochromated Mo K$\alpha$ radiation. All data were corrected for Lorentz, polarization, and absorption effects. Data reduction and analysis were carried out using Kuma Diffraction software.[18] All structures were solved by direct methods and refined by the full-matrix least-squares method on all $F^2$ data, using SHELXTL software.[19] Carbon-bonded hydrogen atoms were included in the calculated positions and refined in the riding mode, using the


dx.doi.org/10.1021/ic402987n | Inorg. Chem. 2014, 53, 1630−1636

**Scheme 1. Synthesis of Chloride-Free $Ba_4Ti_2$-Like Cluster 1**

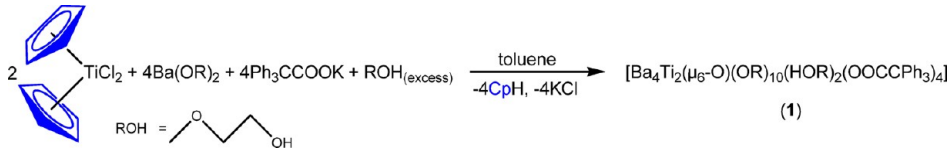


SHELXTL default parameters. Other hydrogen atoms were located in a difference Fourier map, and refined with O−H distance restraints. The coordinated $CH_3OCH_2CH_2OH$ and $CH_3OCH_2CH_2O^-$ molecules were partially disordered, and they were refined in two positions.

**Preparation of Pure $BaTiO_3$.** In a typical procedure, cluster **2** was heated at 800 °C for 1 h in an air atmosphere, at a heating rate of 5 °C $min^{-1}$. After decomposition, the product was identified using powder XRD. In the next step, the raw powder was leached with deionized water and then dried in an oven at 120 °C for 1 h. The morphology and elemental composition of pure $BaTiO_3$ particles were determined using TEM-EDS/SEM-EDS methods. Carbon, hydrogen, and chlorine contaminants were examined using elemental analysis shown in Table S1 (see the Supporting Information) and FT-IR spectroscopy.

**Preparation of Eu-Doped $BaTiO_3$.** Eu-doped samples were synthesized by mixing $BaTiO_3$ derived from **2** with $Eu_2O_3$ and grinding in an alumina mortar with acetone as the wetting medium. The obtained raw powder of $BaTiO_3$:$Eu^{3+}$ was sintered at different temperatures (1000, 1100, and 1300 °C) in an air atmosphere. The Eu concentration was 3 mol % with respect to Ti. The powder XRD patterns of Eu-doped $BaTiO_3$ sintered at different temperatures are shown in Figure S1 (see the Supporting Information); they are in good agreement with those in the ICSD database (ICSD 154344).

## RESULTS AND DISCUSSION

**Syntheses and Thermal Decompositions.** We were interested in developing a method for synthesizing molecular precursors for oxide materials by alcoholysis of chloride transition-metal complexes. We prepared a technologically important group 2/group 4 mixed metal oxide system,[18] barium titanate ($BaTiO_3$), from the organometallic $Cp_2TiCl_2$ and barium alkoxide containing a functionalized bidentate ligand. We used 2-methoxyethanol, because it can easily coordinate in several ways, and it promotes the formation of well-crystallized and soluble compounds in common hydrocarbon solvents.[20]

To avoid the formation of a complex containing $Cl^-$ ligands, we added $Ph_3CCOOK$ to the reaction system. We obtained cyclopentadienyl- and chloride-free $Ba_4Ti_2$-like cluster of formula $[Ba_4Ti_2(\mu_6\text{-}O)(OCH_2CH_2OCH_3)_{10}(HOCH_2CH_2OCH_3)_2(OOCCPh_3)_4]$ (**1**) (Scheme 1).

Single-crystal XRD data showed that solid **1** is a centrosymmetric hexanuclear cluster, with a $Ba_4Ti_2O_9$ core structure and a 2:1 barium/titanium stoichiometry that exactly matches that of spinel (Figure 1). The six metal ions form an octahedron with an interstitial $\mu_6$-O atom and eight $\mu_3$-O bridges. The most probable sources of $O^{2-}$ anions are alkene/ether elimination reactions or adventitious hydrolysis.[21,22] The titanium ions form six-coordinated distorted octahedrons with $O_6$ donor sets, and the barium ions are surrounded by $O_{10}$ donor atoms. The characteristic interatomic distances within the heterometallic core of **1** are given in Tables S2 and S3 in the Supporting Information.

The thermal decomposition of **1** was investigated using TGA-DTA analysis performed in air. A three-step process was observed (Figure 2).The first weight loss occurred below 200 °C and can be ascribed to the removal of residual solvents. This observation was confirmed by an endothermic peak in this temperature region. When the sample was heated to 200−515 °C, the pyrolysis of organic compounds was observed, as indicated by three exothermic peaks in the DTA curve. The third and final weight loss occurred in the temperature region 600−800 °C, and was caused by the decomposition of residual organic and carbonate components. The last exothermic peak at 600 °C was assigned to the formation of $Ba_2TiO_4$. The decomposition of cluster **1** led to a $Ba_2TiO_4$ spinel-like oxide with $BaTiO_3$perovskite impurities. Figure 3 shows XRD patterns of the powders obtained at different sintering temperatures. All patterns were compared with those of

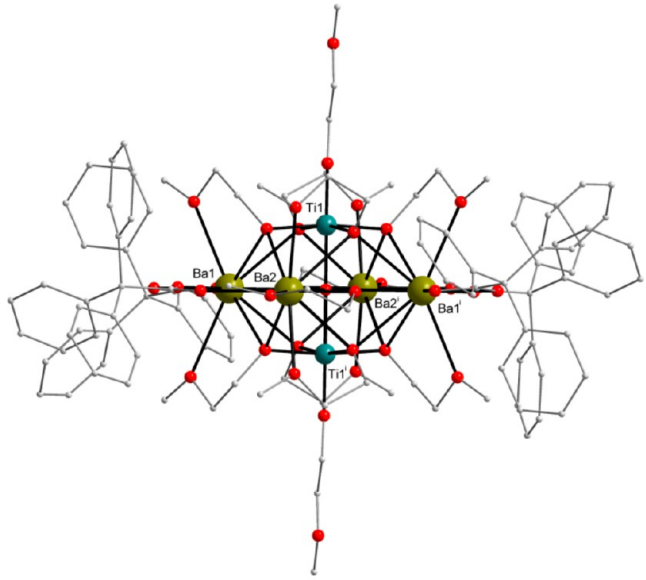


(a)

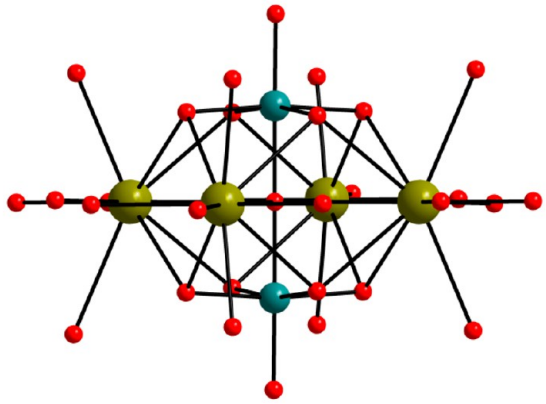

(b)

**Figure 1.** (a) Molecular structure of $[Ba_4Ti_2(\mu_6\text{-}O)(OCH_2CH_2OCH_3)_{10}(HOCH_2CH_2OCH_3)_2(OOCCPh_3)_4]$ (**1**). The second disordered counterparts and hydrogen atoms are omitted for clarity. (b) Central $Ba_4Ti_2(\mu_6\text{-}O)(\mu_3\text{-}O)_8$ core geometry.


dx.doi.org/10.1021/ic402987n | Inorg. Chem. 2014, 53, 1630−1636

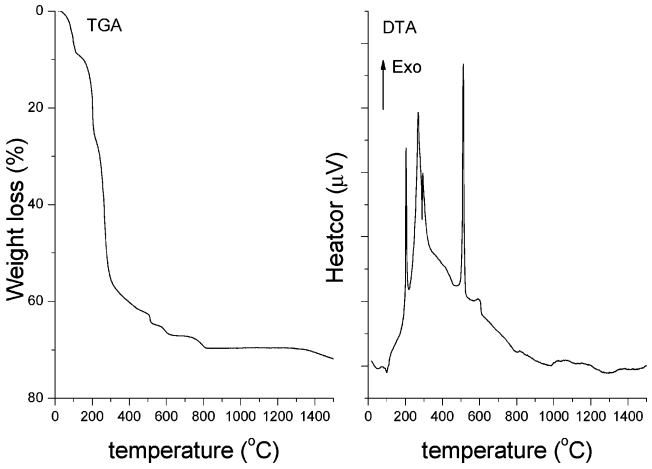


**Figure 2.** TGA and DTA curves of **1**, obtained in air atmosphere.

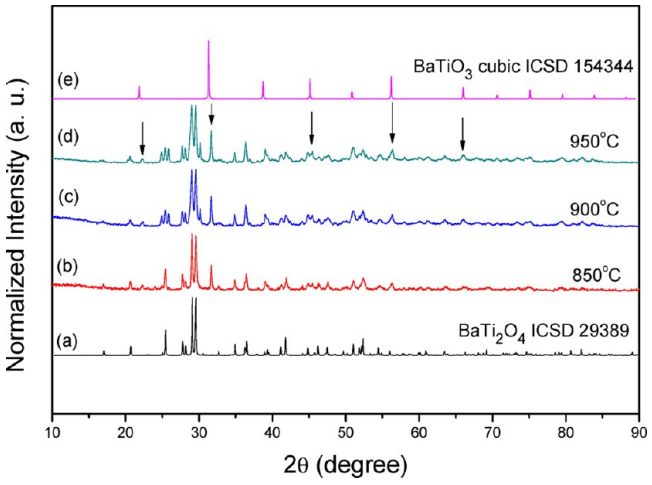


**Figure 3.** Powder XRD patterns: (a) $BaTi_2O_4$ (ICSD 29389), and precursor **1**, sintered at (b) 850 °C, (c) 900 °C, and (d) 950 °C, and (e) cubic $BaTiO_3$ (ICSD 154344).

reference standards for barium titanate and barium orthotitanate. All the $Ba_2TiO_4$ samples obtained were contaminated with $BaTiO_3$. This is also confirmed by the point by point EDS analysis SEM/TEM micrographs (Figure S2 and Table S4 in Supporting Information), which show large crystals of spinel $Ba_2TiO_4$ (Figure 4a,b) coated with small crystals of cubic $BaTiO_3$ (Figure 4c).

Increasing the calcination temperature did not reduce the amount of any of the phases present; therefore, pure $Ba_2TiO_4$ could not be obtained. This is in agreement with the phase diagram of the $BaO-TiO_2$ system,[23] which indicates the presence of perovskite impurities in barium orthotitanate at temperatures up to about 1500 °C. At higher temperatures, $Ba_2TiO_4$ melts, so this approach cannot be used to synthesize the high-purity oxide compound needed for luminescence purposes.

We therefore synthesized a cyclopentadienyl-free heterometallic barium−titanium chloro−alkoxide of composition $[Ba_4Ti_2(\mu_6\text{-}O)(OCH_2CH_2OCH_3)_{10}(HOCH_2CH_2OCH_3)_4Cl_4]$ (**2**). The reaction of $Cp_2TiCl_2$ with 2 equiv of $Ba(OCH_2CH_2OCH_3)_2$ and excess 2-methoxyethanol in toluene at room temperature gave colorless cluster **2** (Scheme 2). In complex **2**, the four triphenyl acetate ligands are substituted by chloride ions. The appearances and molecular structures of **1**

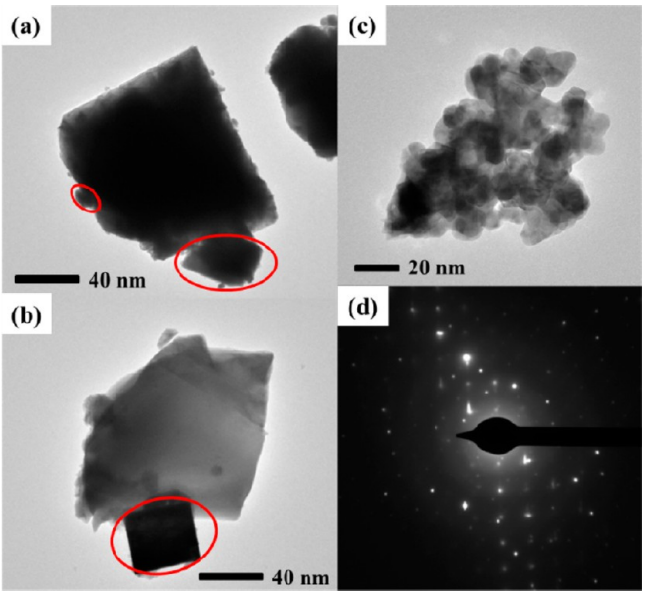


**Figure 4.** (a, b) TEM images of $Ba_2TiO_4/BaTiO_3$ (circled in red), obtained at 900 °C, (c) $BaTiO_3$ crystallites covering spinel surface, and (d) selected area electron diffraction pattern of spinel/perovskite system. The phase composition was confirmed by the EDS analysis (see Supporting Information).

**Scheme 2. Synthesis of Chloride-Containing $Ba_4Ti_2$-Like Cluster 2**

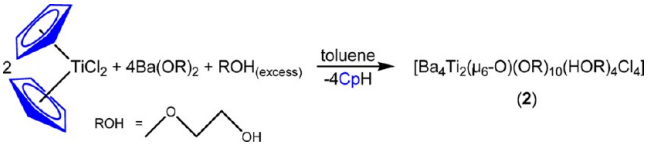


and **2** are similar (compare Figures 1 and 5). The $Ba_4Ti_2(\mu_6\text{-}O)(\mu_3\text{-}O)_8$ core of **2** is an octahedron with six metal centers and a $\mu_6$-oxo encapsulated oxygen atom residing at the central position. We believe that the source of $O^{2-}$ anions is similar to that in cluster **1**. Barium and titanium atoms occupy equatorial and axial positions, respectively. Each of the barium coordination spheres is completed by terminal chloride ligands with a $ClO_8$ donor set. The characteristic interatomic distances and angles of cluster **2** are given in Tables S5−S10 in the Supporting Information.

The thermolysis behavior of **2** is essentially different from that observed for cluster **1** (Figure 6). The key point was to choose appropriate thermolysis conditions. Complex **2** undergoes thermal decomposition at 800 °C to a $BaCl_2/BaTiO_3$ mixture in a 1:1 molar ratio, avoiding the formation of multiphase metal oxide mixtures observed during thermal decomposition of cluster **1**. After barium dichloride has been leached from the raw powder using deionized water (Scheme 3), highly phase-pure particles of composition $BaTiO_3$ (Figure 7), in the size range 80−100 nm, are obtained (Figure 8). The resulting solid $BaTiO_3$ is essentially nonporous to molecular nitrogen, and has a low BET surface area of 8.25 $m^2\ g^{-1}$; this was confirmed by physisorption analysis.

**Luminescence Studies of $BaTiO_3$:Eu.** On the basis of their low porosity and $S_{BET}$ = 8.25 $m^2\ g^{-1}$, we investigated the use of $BaTiO_3$ nanoparticles as a host lattice for lanthanide ions such as $Eu^{3+}$. Low porosity is favorable in phosphors, because


dx.doi.org/10.1021/ic402987n | Inorg. Chem. 2014, 53, 1630−1636

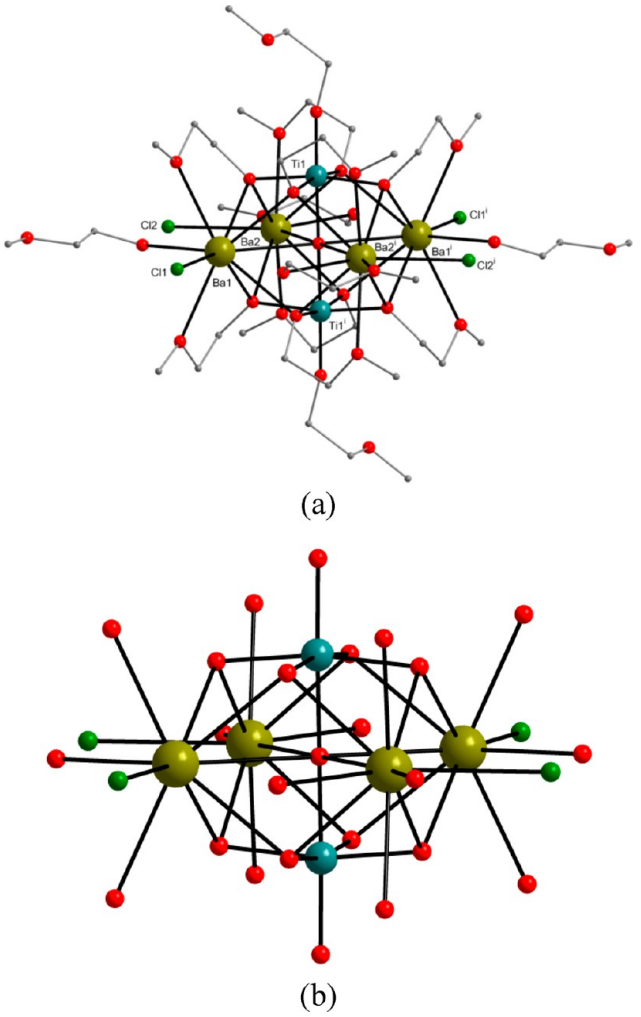


**Figure 5.** (a) Molecular structure of **2** (hydrogen atoms are omitted for clarity) and (b) $Ba_4Ti_2(\mu_6\text{-}O)(\mu_3\text{-}O)_8$ core geometry.

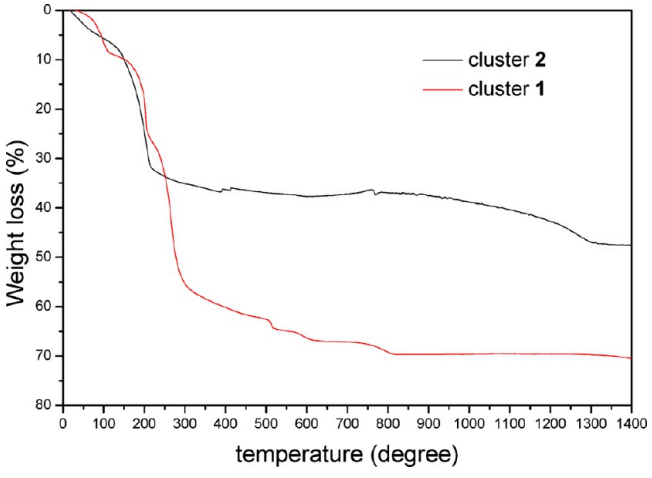


**Figure 6.** Comparison of TGA curves of **1** and **2**.

**Scheme 3. Thermal Transitions of 2 and Separation of Two Phases Using Deionized Water**

$$[Ba_4Ti_2(O)(OR)_{10}(ROH)_4Cl_4] \xrightarrow[\text{-volatiles}]{800\ ^\circ C} 2BaCl_2 + 2BaTiO_3 \xrightarrow[\text{-}2BaCl_2]{\text{de-ionized water}} \underset{\text{white nanopowder}}{2BaTiO_3}$$

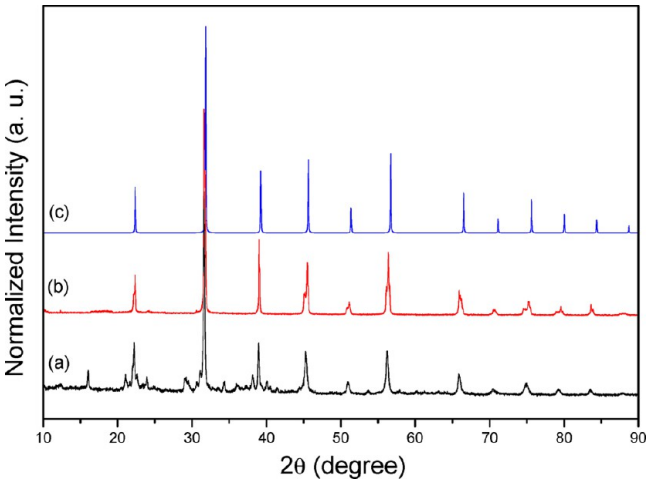


**Figure 7.** Powder XRD patterns: (a) precursor **2** sintered at 800 °C for 1 h, mixture of $BaTiO_3$ and $BaCl_2$, (b) pure $BaTiO_3$ derived from **2**, after leaching, and (c) $BaTiO_3$ (ICSD 154344).

the pores in ceramic microstructures can strongly scatter incident light, making the material opaque.[24]

Figure 9b shows the room-temperature emission spectra of $BaTiO_3$:$Eu^{3+}$ (3 mol %) samples sintered at 1100 °C, obtained at two different excitation wavelengths, i.e., 260 and 393 nm. Both spectra consist of characteristic f−f emission transitions from the $^5D_0$ excited state to the $^7F_J$ ($J$ = 0, 1, 2, 3, 4) ground levels of $Eu^{3+}$. The peak at 617 nm is ascribed to the hypersensitive electric dipole transition $^5D_0$−$^7F_2$, and the peak at 590 nm arises from the magnetic dipole transition $^5D_0$−$^7F_1$. The emission lines at 580, 653, and 704 nm correspond to $^5D_0$−$7F_0$, $^5D_0$−$^7F_3$, and $^5D_0$−$^7F_4$ transitions, respectively. Both spectra are dominated by the electric dipole emission $^5D_0$−$^7F_2$, which is much stronger than the magnetic dipole emission $^5D_0$−$^7F_0$; this leads to the conclusion that $Eu^{3+}$ ions occupy noninversion symmetry sites of cubic-phase $BaTiO_3$.[25] In the cubic cell of barium titanate, $Ti^{4+}$ ions are coordinated by six $O^{2-}$ ligands, and $Ba^{2+}$ ions occupy the center of the cube and are surrounded by 12 $O^{2-}$ ions.[26] Because of the ionic radii of $Ba^{2+}$ (0.135 nm), $Ti^{4+}$ (0.0605 nm), and $Eu^{3+}$ (0.0947 nm),[27] we cannot predict which metal site will be substituted by Eu ions; however, as the sample preparation was performed at high temperatures, it is possible that the $Eu^{3+}$ ions are distributed at both $Ti^{4+}$ and $Ba^{2+}$ sites, as a result of diffusion in the lattice.[17] Decay time of the $^5D_0$ − $^7F_2$ (617 nm) emission was recorded. The luminescence lifetime of the $^5D_0$ level was calculated, giving major value of around 0.61 ms (84%) and minor value of 1.57 ms (16%). The biexponential lifetime could be associated to the possible energy transfer between $Eu^{3+}$ ions due to relatively high dopant concentration and some disorder which affects environment around $Eu^{3+}$ ions.[28] It can be seen that the intensity of the emission for $\lambda_{exc}$ = 260 nm excitation [$Eu^{3+}$−$O^{2-}$ charge transfer (CT)] is much higher than that for $\lambda_{exc}$ = 393 nm ($Eu^{3+}$ f−f transition). This shows that energy transfer from the matrix to the activator is very effective. The excitation spectrum (Figure 9a) corresponding to the 613 nm emission shows a series of narrow peaks in the region from 390 to 550 nm; these peaks are the result of 4f−4f transitions in the $Eu^{3+}$ ions, originating from absorption to $^5L_6$ (391 nm), $^5D_2$ (462 nm), and $^5D_1$ (530 nm) states. The most intense band in the range from 230 to 280 nm corresponds to CT transitions resulting from $Eu^{3+}$−$O^{2-}$ interactions. It can also be seen that


dx.doi.org/10.1021/ic402987n | Inorg. Chem. 2014, 53, 1630−1636

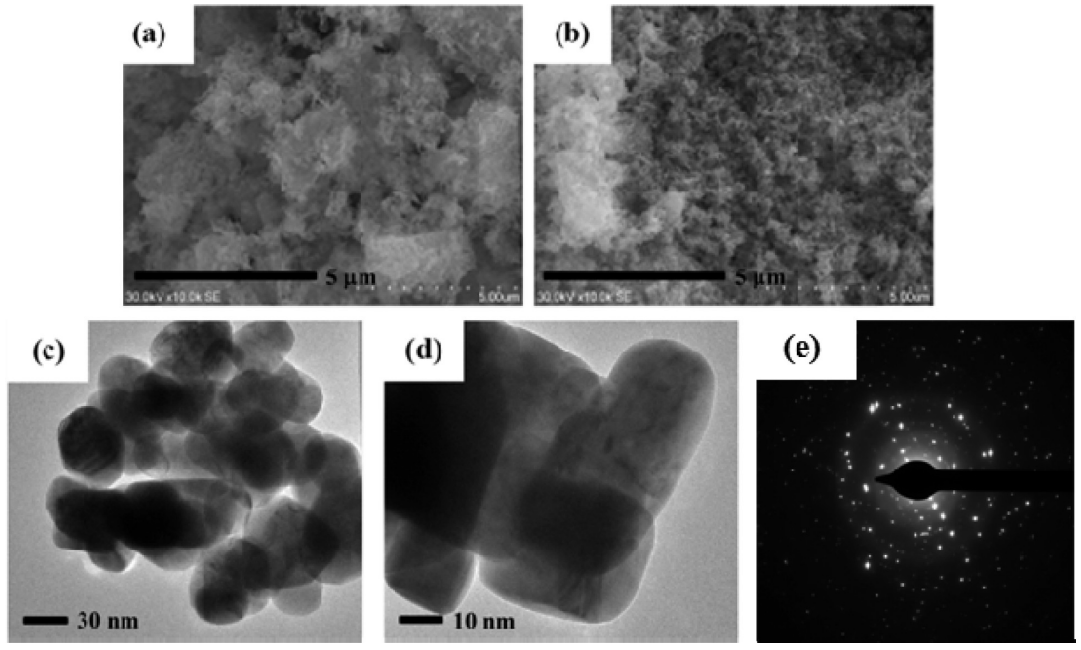


**Figure 8.** (a, b) SEM, (c, d) TEM micrographs, and (e) SAED of $BaTiO_3$ derived from **2**.

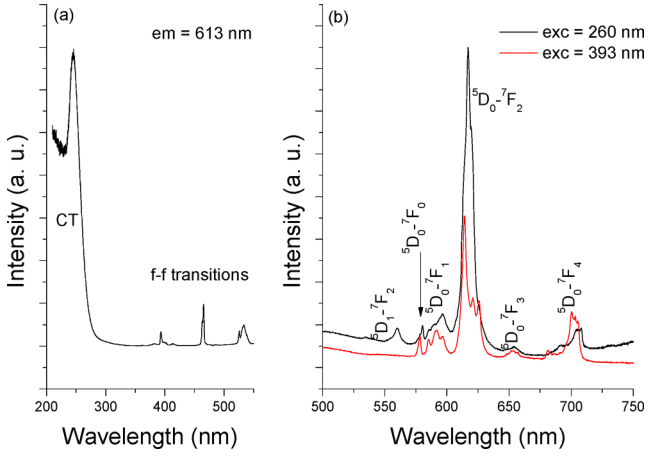


**Figure 9.** Photoluminescence spectra of $BaTiO_3$:$Eu^{3+}$ sintered at 1100 °C: (a) excitation spectrum, $\lambda_{em}$ = 613 nm, and (b) emission spectra recorded at two different excitation wavelengths, $\lambda_{exc}$ = 260 nm and $\lambda_{exc}$ = 393 nm.

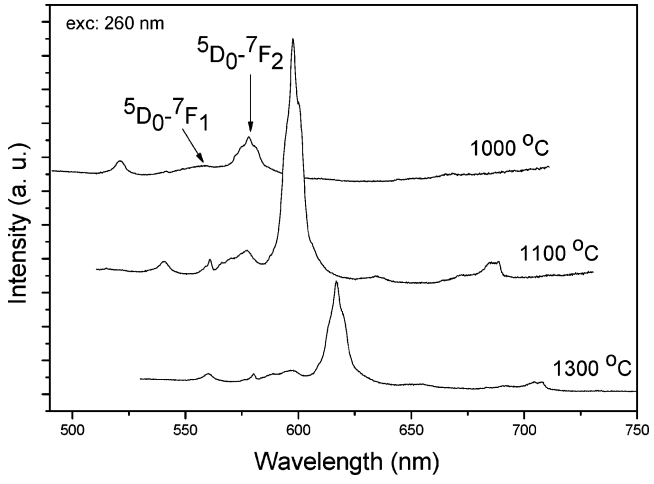


**Figure 10.** Emission spectra ($\lambda_{exc}$= 260 nm) of $BaTiO_3$:$Eu^{3+}$ (3 mol %) sintered at different temperatures: 1000, 1100, and 1300 °C.

the emission spectra change with sintering temperature (Figure 10). The most intense luminescence occurs for the sample sintered at 1100 °C. Increasing the temperature to 1300 °C causes a decrease in the emission intensity. This is because $BaTiO_3$ starts to melt at about 1300 °C, so the luminescence intensity decreases. Melting of the crystalline sample can also be observed in the TEM images (Figure 11).

## CONCLUSIONS

The results of our study demonstrate that molecular precursor **1** cannot be exclusively transformed by thermal decomposition to a pure double-oxide material, and its decomposition always leads to mixture of spinel $Ba_2TiO_4$ and perovskite $BaTiO_3$, despite the fact that the barium/titanium ratio (2:1) at the molecular level should force the formation of spinel-like particles only. This problem, as we expected, was solved by replacing the triphenyl acetate ligands in **1** by chloride ligands.

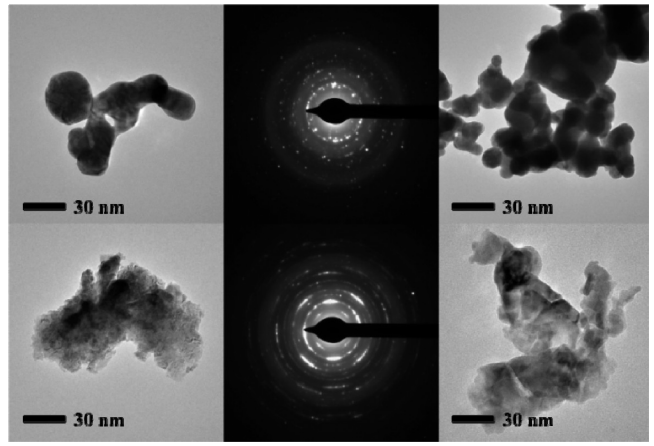


**Figure 11.** TEM images and selected area electron diffraction patterns of $BaTiO_3$:$Eu^{3+}$ sintered at 1000 °C (top) and 1300 °C (bottom).


dx.doi.org/10.1021/ic402987n | Inorg. Chem. 2014, 53, 1630−1636

Furthermore, in a two-step strategy, compound **2** was thermally transformed into a double-phase $BaTiO_3/BaCl_2$ system, and then $BaCl_2$ was easily removed from the raw powder by washing with deionized water. As a result, we obtained pure barium titanate; it is worth noting that we did not observe release of gaseous HCl during thermolysis. Moreover, by using lower temperatures than those used in conventional solid-state thermal routes involving carbonate/oxide mixtures, we easily transformed complex **2** into a highly phase-pure binary oxide $BaTiO_3$ material, which was used in the next stage of our studies as a host matrix for Eu-doped phosphors.

## ■ ASSOCIATED CONTENT

### Supporting Information

Powder XRD patterns of Eu-doped $BaTiO_3$ sintered at different temperatures, and full crystallographic data of **1** and **2**, including CIF data. This material is available free of charge via the Internet at http://pubs.acs.org.

## ■ AUTHOR INFORMATION


### Corresponding Author

*E-mail: piotr.sobota@chem.uni.wroc.pl.



### Funding

### Notes

The authors declare no competing financial interest.


## ■ ACKNOWLEDGMENTS


The authors would like to express their gratitude to the National Science Centre (Grants 2011/03/B/ST5/01040 and 2011/01/N/ST5/02408) for financial support.


## ■ REFERENCES


(1) Wright, P. J.; Anthony, C. J.; Crosbie, M. J.; Donohue, P. P.; Lane, P. A.; Todd, M. A. *J. Mater. Chem.* **2004**, *14*, 3251−3258.
(2) Seisenbaeva, G. A.; Kessler, V. G.; Pązik, R.; Stręk, W. *Dalton Trans.* **2008**, 3412−3421.
(3) McElwee-White, L. *Dalton Trans.* **2006**, 5327−5333.
(4) Hubert-Pfalzgraf, L. G. *J. Mater. Chem.* **2004**, *14*, 3113−3123.
(5) Jones, A. C. *J. Mater. Chem.* **2002**, *12*, 2576−2590.
(6) Epifani, M.; Andreu, T.; Arbiol, J.; Díaz, R.; Siciliano, P.; Morante, J. R. *Chem. Mater.* **2009**, *21*, 5215−5221.
(7) Epifani, M.; Imperatori, P.; Mirenghi, L.; Schioppa, M.; Siciliano, P. *Chem. Mater.* **2004**, *16*, 5495−5501.
(8) Epifani, M.; Andreu, T.; Magana, C. R.; Arbiol, J.; Siciliano, P.; D'Arienzo, M.; Scotti, R.; Morazzoni, F.; Morante, J. R. *Chem. Mater.* **2009**, *21*, 1618−1626.
(9) Nunes, G. G.; Kessler, V. G. *Inorg. Chem. Commun.* **2006**, *9*, 667−670.
(10) Kessler, V. G.; Seisenbaeva, G. A.; Errington, R. J. *Inorg. Chem. Commun.* **2005**, *8*, 503−505.
(11) Hamid, M.; Tahir, A. A.; Mazhar, M.; Zeller, M.; Hunter, A. D. *Inorg. Chem.* **2007**, *46*, 4120−4127.
(12) Mishra, S.; Jeanneau, E.; Berger, M.-H; Hochepied, J.-F.; Daniele, S. *Inorg. Chem.* **2010**, *49*, 11184−11189.
(13) Jaglinski, T.; Kochman, D.; Stone, D.; Lakes, R. *Science* **2007**, *315*, 620−622.
(14) Nalwa, H. S. *Handbook of Low and High Dielectric Constant Materials and their Applications*; Academic Press: New York, 1999.
(15) Wadhan, V. K. *Introduction to Ferroic Materials*; CRC Press: Boca Raton, FL, 2000; p 10.
(16) Tang, P.; Towner, D.; Hamano, T.; Meier, A.; Wessels, B. *Opt. Exp.* **2004**, *12*, 5962−5967.
(17) Patel, D. K.; Vishwanadh, B.; Sudarsan, V.; Vatsa, R. K.; Kulshreshtha, S. K. *J. Am. Ceram. Soc.* **2011**, *94*, 482−487.
(18) *CrysAlis CCD and CrysAlis RED, Versions 1.171.33*; Oxford Diffraction Poland: Wrocław, Poland, 2009.
(19) *SHELXTL, Version 6.14*; Bruker AXS, Inc.: Madison, WI, 2003.
(20) (a) Drąg-Jarząbek, A.; Kosińska, M.; John, Ł.; Jerzykiewicz, L. B.; Sobota, P. *Chem. Mater.* **2011**, *23*, 4212−4219. (b) Sobota, P.; Drąg-Jarząbek, A.; Utko, J.; Jerzykiewicz, L. B. *Organometallics* **2011**, *30*, 1741−1743. (c) Sobota, P.; Drąg-Jarząbek, A.; John, Ł.; Utko, J.; Jerzykiewicz, L. B.; Duczmal, M. *Inorg. Chem.* **2009**, *48*, 6584−6593. (d) Sobota, P.; Utko, J.; John, Ł.; Jerzykiewicz, L. B.; Drąg-Jarząbek, A. *Inorg. Chem.* **2008**, *47*, 7939−7941. (e) Utko, J.; Ejfler, J.; Szafert, S.; John, Ł.; Jerzykiewicz, L. B.; Sobota, P. *Inorg. Chem.* **2006**, *45*, 5302−5306.
(21) Clayden, J. *Nat. Chem.* **2010**, *2*, 523−524.
(22) Turova, N. Yu.; Turevskaya, E. P.; Kessler, V. G.; Yanovsky, A. I.; Struchkov, Y. T. *J. Chem. Soc., Chem. Commun.* **1993**, 21−23.
(23) Moulson, A. J.; Herbert, J. M. In *Electroceramics: Materials, Properties, Applications*; John Wiley & Sons Ltd.: Chichester, U.K., 2003.
(24) Ji, Y.; Jiang, D. Y.; Chen, J. J.; Qin, L. S.; Xu, Y. P.; Feng, T.; Shi, J. L. *Opt. Mater.* **2006**, *28*, 436−440.
(25) Stręk, W.; Hreniak, D.; Boulon, G.; Guyot, Y.; Pązik, R. *Opt. Mater.* **2003**, *24*, 15−22.
(26) Lu, D.; Ogata, T.; Unuma, H.; Li, X.; Li, N.; Sun, X. *Solid State Ionics* **2011**, *201*, 6−10.
(27) Lide, D. R.; Frederikse, H. P. R. *CRC Handbook of Chemistry and Physics*; CRC Press: Boca Raton, FL, 1996; p 12-4.
(28) Pązik, R.; Wiglusz, R. J.; Stręk, W. *Mater. Res. Bull.* **2009**, *44*, 1328−1333.